Disrupting Cdc42 Activation-Driven Filopodia Formation with Low-Intensity Ultrasound and Microbubbles: A Novel Strategy to Block Ovarian Cancer Metastasis

Xiaoying Li[1], Chengwei Tan[2], Xiuxiu Fu[2], Jian Qiu[3], Wanting Shen[2], Zhikang Xu[2], Xiaodong Wu[2], Yiting Zhou[4]✉, Xiao Li[2]✉, Litao Sun[1]✉, Jiale Qin[2,5,6]✉

[1] Cancer Center, Department of Ultrasound Medicine, Zhejiang Provincial People's Hospital (Affiliated People's Hospital), Hangzhou, 310006, China

[2] Women's Hospital, Zhejiang University School of Medicine, Hangzhou, 310006, China

[3] Department of Obstetrics and Gynaecology, Huzhou Central Hospital, Affiliated Central Hospital Huzhou University, Huzhou, 313000, China

[4] Department of Orthopaedic Surgery and Department of Biochemistry of the Second Affiliated Hospital, Liangzhu Laboratory, Zhejiang University School of Medicine, Hangzhou, 310058, China,

[5] Zhejiang Key Laboratory of Precision Diagnosis and Therapy for Major Gynecological Diseases, Hangzhou, 310006, China

[6] Zhejiang Provincial Clinical Research Center for Gynecological and Obstetrical Diseases, Hangzhou, 310006, China

✉corresponding authors: qinjiale@zju.edu.cn, sunlitao@hmc.edu.cn, 5198008@zju.edu.cn, and zhouyt@zju.edu.cn

Abstract:

Introduction: Metastasis is a leading cause of mortality and treatment failure in ovarian cancer. However, effective strategies to target this process remain limited. Low intensity ultrasound (LIUS) and microbubbles (MBs) have shown promise in blood-brain barrier opening and drug delivery. However, the role in tumor metastasis remains unexplored. **Objectives:** To investigate the potential of LIUS and MBs in inhibiting ovarian cancer metastasis and the underlying mechanisms. **Methods:** Based on the results of cell experiments to identify the optimal parameters, three ditinct mouse models-orthotopic, intraperitoneal metastatic, and hematogenous metastatic nude mouse models-were established to evaluate the spatiotemporal effects of LIUS and MBs on ovarian cancer metastasis. Filopodia and lamellipodia formation in cancer cells was assessed using both immunofluorescence and scanning electron microscopy. Additionally, the expression levels of total Cdc42 and active Cdc42 were measured. Finally, the constitutively active Cdc42 rescue experiment was performed. **Results:** Our results demonstrated that LIUS and MBs significantly suppressed metastasis in orthotopic ovarian cancer, as well as individually reducing both intraperitoneal and hematogenous metastatic potential in treated cells. This treatment was associated with a reduction in the length and number of filopodia, while the number of lamellipodia remained unaffected. Notably, this is the first study conducted at the molecular level to demonstrate that the disturbing of filopodia by LIUS and MBs is mediated through the modulation of Cdc42 activation. In this, the inhibitory effect of LIUS and MBs on both filopodia formation and the metastatic potential of ovarian cancer cells was reversed by the overexpression of constitutively active Cdc42. **Conclusion:** Our findings indicated that LIUS and MBs possesses the capacity to inhibit tumor metastasis via disturbing the cytoskeletal remodelling of filopodia. This study provides novel insights into the mechanisms underlying the metastatic inhibition by LIUS and MBs, expanding the understanding of this technique beyond its established uses.

Keywords: Low intensity ultrasound, ovarian cancer, metastasis, filopodia, Cdc42

1. Introduction

The considerable mortality rate of ovarian cancer, having a five-year survival rate of 30-50%, poses a severe threat to women's health [1, 2]. Standard first-line therapy involves cytoreductive surgery in conjunction with platinum-based chemotherapy and maintenance therapy (NCCN Guidelines ®) [3]. However, the presence of unresectable lesions during debulking surgery, as opposed to when complete resection is possible, leads to higher rates of local and distant metastasis and recurrence. Both aspects of metastasis serve as independent risk factors for poor prognosis [2, 4]. In such cases, the development of effect adjuvant therapy to inhibit the metastasis of these unresectable residual lesions is suggested to represent the most direct and effective approach.

Ultrasound therapy strategies that harness the mechanical activity of ultrasound stimulate the microbubbles (MBs) for bioeffects are being actively developed [5]. Gas-filled MBs are highly sensitive to changes in pressure, due to this, their volume can change rapidly and dramatically when they are exposed to ultrasonic waves. These volume changes act on cells or tissues can induce mechanical effects, chemical effects, and thermal effects [5]. It is worth noting that the biological effects induced by different ultrasonic parameters are also very different. Low intensity ultrasound (LIUS) interaction with MBs minimize thermal effects, and the mechanical effects caused by them are mainly cavitation and secondary effects, including direct impingement, ballistic motion, and microstreaming [5, 6]. Furthermore, the allure of LIUS therapy stems from its ability to treat deeply situated tumors within the body effectively without causing significant harm to the overlying skin and adjacent normal tissues [7]. The most developed application of LIUS stimulated MBs is drug delivery, as the bioeffects caused by the interaction between LIUS and MBs are gradually studied, increasing attention is being paid to their role in tumor therapy.

LIUS combined with MBs, as a potential adjuvant therapy, is known to provide an additional suppressive impact against tumor metastasis [8]. An extensive array of laboratory animal studies have demonstrated that the amalgamation of LIUS and MBs with chemotherapy [8, 9], immunotherapy [10], or drug carriers [11], can thereby significantly curtail tumor metastasis. Clinical trials have also been implemented utilizing LIUS-triggered MBs to augment chemotherapy for pancreatic cancer [12, 13] and gastrointestinal malignancies [14]. In these examples tumor progression was restricted to the original sites with no emergence of new lesions [12-14]. Another

recent *in vitro* study has also provided new evidence that LIUS can impede the collective migration of pancreatic cancer cells [15]. Unfortunately, there have been no *in vivo* studies to date that examine the direct inhibitory effects or mechanisms of LIUS combined with MBs on tumor metastasis. In this study, we explored the inhibitory effect of LIUS and MBs on ovarian cancer metastasis *in vivo* via the constructing orthotopic ovarian cancer, peritoneal metastasis, and hematogenous metastasis nude mouse models.

At the mechanistic level, similar to other cancers, ovarian cancer metastasis involves a series of multistep cellular processes known as the invasion-metastasis cascade [16, 17]. Filopodia, at the leading edge of tumor cells, play an important role in this by determining the direction of cell movement in the initiation of tumor cell migration [17, 18]. The development and protrusion of filopodia towards signaling sources are regulated by dynamic processes of cytoskeletal remodeling which are regulated by the small GTPase Cdc42 signaling pathway. The activation of Cdc42 is due to the phosphoric acid group of GTP binding to the carboxyl group of Cdc42 protein. After this Cdc42 interacts with downstream effector proteins to direct the assembly of actin-based structures and stimulate the formation of filopodia [19-21]. Here, we speculate that the diminished capacity for cellular migration and invasion can be attributed to the reduction in filopodia development resulting from LIUS-triggered MBs-induced inhibition of Cdc42 activity.

In summary, elucidating the inhibitory effects of LIUS combined with MBs on ovarian cancer metastasis and its underlying mechanisms will provide a scientific basis for considering LIUS as an adjuvant therapeutic strategy for the prevention and treatment of ovarian cancer metastasis.

2. Materials and methods

2.1 Cells and reagents

The human epithelial ovarian cancer lines SKOV3 (CS-K8752X), HO8910PM (CS-K8752X) and ovarian epithelial cell line IOSE80 (CS-K88024X) that has been immortalized but is not tumorigenic were purchased from the Shanghai C-reagent Biotechnology Co. Ltd. (Shanghai, China). SKOV3, HO8910PM, and IOSE80 were grown in a mixture of RPMI 1640 medium (BC-M-017, Biochannel, China), which were supplemented with 10% fetal bovine serum (FBS) (BC-SE-FBS01, Biochannel, China) and 1% streptomycin and penicillin. By transducing luciferase-

expressing lentivirus constructs of SKOV3-luc cells (Shanghai C-reagent Biotechnology Co. Ltd., Shanghai, China) were cultured in RPMI 1640 completed medium. Cell culturing was performed in an atmosphere of 5% CO_2 at 37°C.

2.2 Ultrasound treatment procedure

A single element planar ultrasound transducer, driven by a power source host, was used to generate ultrasound pulses (Chongqing Ronghai Ultrasound Medical Engineering Research Center Co., Ltd.). The transducer had a center frequency of 1.03MHz, a diameter of 35mm, and was held in place using a gripping device. The pulse repetition frequency was 2360Hz. Three minutes of ultrasound were applied to cells suspensions (duty cycle = 20%). The acoustic contrast agent SonoVue® (Bracco, Milan, Italy) as MBs was used to induce cavitation. The SonoVue® MBs was prepared as a suspension in-situ via mixing the powder with 5ml of sterile saline in accordance with the manufacturer's instructions. Our MB/cell ratio was maintained at around 100/1 according to Song et al. 's study [22]. For exposure to LIUS and MBs treatment, the sample cells were plated in 35mm dish and the dish was aligned axially with the ultrasound transducer.

2.3 Lentiviruses, plasmids, and transfection

Lifeact-mcherry overexpression lentivirus (Ubi-MCS-SV40-puromycin) was synthesized by Genechem (China). Transfection was performed with Lipofectamine 3000 (L3000015, Thermo Fisher Scientific, USA). The pXJ40-HA-Cdc42CA (constitutively activate Cdc42, G12C mutation) was received as a kind gift from Prof. Yiting Zhou (Zhejiang University, China). An empty pXJ40-HA vector was used as a control. The plasmids were transfected using Lipofectamine 3000 (L3000015, Thermo Fisher Scientific, USA).

2.4 Cell viability assays

Based on the manufacturer's instructions, the viability of SKOV3 was assessed using the Calcein-AM/ Propidium Iodide (PI) double staining kit (40747ES76, Yaseen, China) [23]. Specifically, 5 μL of Calcein-AM (2 mM) and 15 μL of PI (1.5 mM) were diluted in 5 mL of 1× assay buffer and subsequently applied to SKOV3 cells following the LIUS and MBs treatment. After a 30-minute incubation period, phosphate-buffered saline (PBS) was used to rinse the stained cells and washed

twice before flow cytometry detection.

2.5 Wound healing assay

Our wound healing assays were conducted using 6-well plates with 4 well culture insert (#80469, Ibidi, Germany) [24]. The cells were cultured by seeding them into above plates after with or without LIUS and MBs treatment, the cell concentration was adjusted to 110 μl of cell suspension (SKOV3 3×10^5 cells/ml, HO8910PM 1×10^6 cells/ml). A culture of the cells was performed overnight, and the inserts were removed. Following the removal of non-viable cells using PBS, the remaining cells were maintained in RPMI 1640 culture medium with 2% FBS. Each wound was documented through photography (CKX53, Olympus, Japan) at the specified time points. The wound closure rate was subsequently calculated using Image J software.

2.6 Transwell migration and invasion

For transwell assays, 6.5mm-diameter transwell plate inserts with 8 μm pore size (#3421, Corning, NY, USA) were used [25]. An upper chamber of a transwell plate was seeded with a serum-free medium containing 200 microliters of cell suspension (SKOV3 5×10^5 cells/ml, HO8910PM 2.5×10^6 cells/ml) with or without LIUS and MBs. Lower chambers were enriched with 10% FBS in 500μl RPMI 1640 medium. Cells were then cultured for 24 hours as described above. A matrigel-coated (#356234, Corning, USA) upper chamber was used for invasion experiments. The cells on the inner side of the upper chamber were then removed using cotton swabs, and 4% paraformaldehyde was used to fix the cells on the upper chamber migrated to lower surface of the membrane and stained them with crystal violet (BL539A, Biosharp, Beijing, China) for observation and counting under a microscope (CKX53, Olympus, Japan). Number of cells that migrated was counted in 5 different fields and results were determined from three repeated experiments.

2.7 Western blot

We performed Western blot analysis in accordance with the previous description [26]. A cocktail of protease inhibitors has been added to RIPA buffer (P0013, Beyotime, China) to facilitate cell lysis. The samples were subsequently run on 4-20% gels (IPVH00010, GenScript, China), and then the proteins were transferred onto PVDF membranes (IPVH00010, Millipore, USA). The

membranes were blocked with 5% non-fat milk and then incubated overnight at 4°C with primary antibodies. Thereafter, secondary antibodies conjugated to HRP were incubated for 1 hour at room temperature. Chemiluminescence reagents were used to visualize Western blots analysis (WBKLS0100, Millipore, USA). Proteins were detected using Azure biosystems (Azure 500, USA). Primary antibodies used were anti-Cdc42 (1:10000; AB187643, Abcam, USA) and anti-GAPDH (1:10000; AB181602, Abcam, USA). Secondary antibodies were purchased from Biodragon (1:10000, BF03116, China).

2.8 Live-Cell Imaging

SKOV3-lifeact-mcherry cells fluorescently labeled with red F-actin were used for time-lapse microscopy. The cells were incubated in a 6-well plate at a suitable density the night before observation, and the nuclei were labeled with Hoechst (33342, Thermo Fisher Scientific, USA). Observations were made immediately after LIUS and MBs treatment and continued for 6 h, with time-lapse images were acquired at 5 min per frame. The sites of all cells were recorded and used to plot trajectories. The Imaris software was used to calculate the accumulated distance, Euclidean distance, average cell velocity, and directionality for each group. The Euclidean distance is defined as the distance between first and last position of cell motility. The accumulated distance is the total length of the cell's trajectory. The average cell velocity on an orbit is divided by the cumulative distance divided by the time it takes the cell to travel that distance. Cell movement directivity is defined as the ratio of Euclidean distance to cumulative distance. The persistence of cell movement in a preferred direction is assessed by calculating the directionality of each cell. A directionality value of 1 indicated that the cells moved in a straight line.

2.9 Scanning electron microscopy

Scanning electron microscope (SEM) observations were performed on Nova Nano SEM (NNS-450). SEM measurements were conducted at 500 kV, with a resolution of up to 1.4nm. SKOV3 cells were analyzed using SEM after being treated with ultrasonic cavitation 6h or untreated.

2.10 Immunofluorescence assay

SKOV3 cells (1×10^5) were seeded in 35mm glass-bottom dish (Biosharp, China). After LIUS and MBs treatment, cells were washed with PBS 3 times, and fixed with 4% paraformaldehyde for 10

min. Then the cells were permeated by 0.3% Triton X-100 for 10 min. After the cells were sealed by 5% BSA for 30 min, they were incubated at 4°C overnight with F-actin antibodies (ab205, Abcam, USA). The secondary antibody was used Rhodamine-linked Anti-mouse IgG (SA00007-1, Proteintech, Chian). Following 1 h of incubation at room temperature and then stained with DAPI antifade solution (C1006, Beyotime, China). A confocal microscope (Leica, Germany) was used to capture fluorescence images.

2.11 RNA Sequencing

RNA sequencing was conducted by Shanghai Model Organisms Center (Shanghai, China). In summary, the collected SKOV3 cells which after treated with ultrasonic cavitation 3h, 6h, 12h, and 24h and non-treatment RNA isolation utilizing TRIzol reagent (Invitrogen). Subsequently, ribosomal RNA (rRNA) was removed from total RNA using the TruSeq Stranded Total RNA with Ribo-Zero Gold kit, followed by reverse transcription to synthesize complementary DNA (cDNA). The purified DNA was then amplified through polymerase chain reaction (PCR) and subjected to quality assessment using the Agilent Bioanalyzer 2100 system (Agilent Technologies, USA). Finally, an Illumina sequencer was utilized for sequencing.

2.12 Proteomics

A proteomics study was conducted by Oebiotech LTD (Shanghai, China) which contained normalized protein expression data in the mass spectrometry from the SKOV3 cell after LIUS and NBs treatment 6h, 12h and 24h and non-treatment.

2.13 Cdc42 Pull-Down activation assay

Active Cdc42 level was assessed by a Cdc42 Pull Down activation assay kit (#80701, NewEast Biosciences, PA, USA) which selectively recognizes Cdc42GTP [27]. SKOV3 cells were post treated by ultrasonic cavitation for 6h and subsequently collected and subjected to lysis. Cellular protein lysates underwent incubation with a monoclonal antibody specific to active Cdc42 (#26905, NewEast Biosciences, PA, USA), which selectively recognizes Cdc42GTP. The Cdc42GTP complex was then pulled down using protein A/G agarose (#30301, NewEast Biosciences, PA, USA) at 4 °C for 1 hour with agitation by sample mixer. Following centrifugation, washing, and

resuspension in 2x SDSPAGE protein loading buffer. After boiling for 5 minutes, the lysate-antibody complex was eluted from the agarose. The proteins were then analyzed through immunoblotting using an anti-Cdc42 antibody (#21010, NewEast Biosciences, PA, USA) after electrophoresis and membrane transfer.

2.14 Animal studies

The animal experiments in this study were reviewed and approved by the ethics committee of the Zhejiang Chinese Medical University Laboratory Animal Research Center (Hangzhou, China). Institutional and Animal Care and Use Committee guidelines were followed in the care and handling of the animals (No. 20230911-11). The 4-week-old BALB/c female nude mice were purchased from Shanghai BK Lab. Animal Research Center (Shanghai, China).

For orthotopic ovarian cancer nude mouse models, 2×10^6 SKOV3-luc cells were injected into the right ovary of the nude mice. *In vivo* imaging system (IVIS) imaging was performed 10 days after SKOV3-luc cell injection. The mice were randomly divided into two groups (one group for LIUS + MBs treatment, the other group untreated), with each group consisting of 6 mice. Ultrasonic cavitation treatment group followed with acoustic intensity = 0.6 W/cm^2; duty cycle =20%; exposure time = 5 min; caudal vein administration of 200uL microbubbles per mouse, and with treatment administered every other day. On Day 31, the mice were killed, and tumor tissues were harvested.

For nude mice of the ovarian cancer, peritoneal metastasis, and hematogenous metastasis models, those were injected SKOV3-luc cells in the abdomen or caudal vein. In these 2×10^6 SKOV3-luc cells were subjected to ultrasonic cavitation treatment (acoustic intensity = 0.6 W/cm^2; duty cycle =20%; exposure time = 3 min, maintaining the microbubble /cell ratio at around 100/1) which is the ultrasonic cavitation group. The nude mice of the control group were injected 2×10^6 SKOV3-luc cells without any treatment in the abdomen or caudal vein. 6 mice were treated in each group. IVIS imaging was then performed on 10, 17, 24, 31 days. On Day 31, the mice were killed, and tissues were harvested.

Animals were monitored once a week using the IVIS Spectrum in vivo imaging system (PerkinElmer) for luciferase signal detection. IVIS images were captured to assess the bioluminescence signal. The specific procedure is as follows: Nude mice were intraperitoneally

injected with the luciferase D-luciferin potassium luminescent substrate (122799, PerkinElmer, USA) at a concentration of 30 mg/mL, with each mouse receiving 100 μL. Five minutes post-injection, the mice were placed in a transparent plexiglass anesthesia chamber (3.5% isoflurane). After achieving anesthesia, the mice were transferred to the imaging system. Automatic exposure is used for imaging.

2.15 Statistical analysis

This study was conducted using Graphpad Prism 10.0 for statistical analysis (GraphPad Software, USA). Data is expressed as mean and standard deviation. The difference between groups was analyzed statistically using Student's t-tests. For multiple comparisons, one-way analysis of variance (ANOVA) was used. If the data did not follow a normal distribution, non-parametric tests were applied as appropriate. Statistics were considered significant if the difference was $p < 0.05$.

3. Results

3.1 LIUS combined with MBs reduced ovarian cancer cell migration and invasion

Based on the significant differences in cell characteristics (e.g., stiffness) and morphology (e.g., nuclear size) between cancer and normal cells, as well as the distinctive spectral differences in their inherent vibration frequencies, selectively targeting cancer cells for disruption using LIUS has been proposed [28]. Our previous research found that Low-Intensity Focused Ultrasound induced MBs could reverse paclitaxel resistance in ovarian cancer via inhibiting autophagy [29]. The degree of lethal cell injury induced by LIUS and MBs correlated with exposure intensity [30, 31]. In this study, cell viability rates were measured by the flow cytometry analyses after LIUS and MBs on normal ovarian epithelial cells (IOSE80 cells). Results showed that the cell mortality rate began to exceeded 10% when the LIUS intensity was 1.8 W/cm^2. Conversely, when the LIUS intensity was below 1.0 W/cm^2, no significant difference in cell mortality was observed before and after LIUS and MBs treatment (Fig. 1A). To avoid damaging non-cancerous cells, tissues, or organs, it is therefore becoming necessary to choose an appropriate ultrasonic intensity with a mortality rate of less than 10% [32-34]. Wound healing assays were then used to observe the inhibitory levels at varying LIUS (0.2 W/cm^2 -1.0W/cm^2) and MBs upon the migration of ovarian cancer SKOV3 (Fig. 1B) and HO8910PM (Fig. S1). The inhibitory effect of LIUS combined with MBs on SKOV3 cell

migration was found to be intensity-dependent. At an ultrasound intensity of 0.2 W/cm², no significant difference in cell migration was observed between the LIUS + MBs-treated and untreated groups. However, at 0.6 W/cm², a clear inhibitory effect on ovarian cancer cell migration was observed. The inhibitory effect was even more pronounced at an intensity of 1.0 W/cm² (Fig. 1B). In the case of HO8910PM cells, no significant inhibition of cell migration was observed with LIUS + MBs at 0.2 W/cm². At 0.6 W/cm², a significant reduction in cell migration was observed, and a similar effect was noted at 1.0 W/cm², and no obvious ultrasonic intensity dependence was shown (Fig. S1). This suggests that the inhibitory effect of LIUS combined with MBs on ovarian cancer cells exhibits cellular heterogeneity. Further, the transwell assay was employed to further explore the influence of LIUS with 0.6 W/cm^2 on migration and invasion of ovarian cancer cells. Results showed a clear decrease in migratory and invasion capacity of SKOV3 (Fig. 1C, D) and HO8910PM (Fig. S2A, B) cells that had received LIUS and MBs treatment.

To observe the real-time inhibitory effect of LIUS and MBs treatment on single cell motility, time-lapse microscopy was employed to capture the trajectory of SKOV3 cell movement (Fig. S3A). To measure these differences in cell migration, individual cells were tracked for 6 hours, and representative migration tracks of 180 cells from both the untreated and treated (LIUS + MBs) groups were recorded. Subsequently, a quantitative analysis of these cell migration patterns was performed to characterize their migratory properties. Cells treated with LIUS and MBs showed significantly lower migration velocities and shorter migration distances (including accumulated distance and Euclidean distance (Fig. S3B-D)). Additionally, following LIUS + MBs treatment, the orientation of the cells was reduced (Fig. S3E). Here, 'orientation' refers to the persistence of movement in a preferred direction. Tumor cell directional movement plays a crucial role in metastasis, influencing the spread and growth of cancer [35]. These results suggested that LIUS combined MBs not only affected cell motility but may also interfered with the direction of tumor cell movement. Markedly decreased cell migration and invasion was noted after LIUS and MBs treatment, compared to that of non-treatment group. Considering the above results, we chose the minimum effective LIUS intensity 0.6 W/cm^2 for the subsequent *in vivo* experiments.

3.2 LIUS combined with MBs reduced the tumorigenicity and metastasis in an orthotopic ovarian cancer mouse model

The orthotopic mouse tumor model implants tumor cells or tissue into the correct anatomical site, closely replicating the tumor's natural growth environment. This approach more accurately reflects the biological characteristics of tumors, and since tumor growth and metastasis in this model resemble human conditions, it offers clinically relevant insights for evaluating therapeutic efficacy [36]. To examine the effect of LIUS and MBs treatment on tumor tumorigenicity and metastasis *in vivo*, an ovarian cancer orthotopic transplantation model was constructed (Fig. 2A). To monitor tumor growth of ovarian cancer, an *in vivo* imaging system (IVIS) was used to visualize fluorescence intensity (Fig. 2B). Subsequently, the fluorescence intensity was quantified. Building upon previous research on LIUS with MBs methods [22, 37], this study adopts a regimen of 10 sessions, each lasting 5 minutes, conducted every other day using LIUS and MBs. As displayed in Fig. 2C, the average total luminescence flux for treated mice was significantly decreased after treating with LIUS and MBs 10 sessions of 5 minutes every other day. There was no significant difference in fluorescence intensity between the LIUS + MBs treated group and the control (untreated) group on days 10, 17, and 24 after tumor inoculation. This suggested that LIUS + MBs therapy may require multiple repetitions. Abdominal metastases in mice were then assessed through macroscopic observation, and the number of metastases was significantly less in the LIUS and MBs treatment group compared (Fig. 2D, E). Two of six control (no LIUS and MBs treatment) mice developed metastases, however, no instances of metastasis were observed in the LIUS and MBs treatment group. There was no significant difference in the number of metastatic mice between the two groups (Fig. S4). It was possible that the sample size was insufficient to yield more meaningful statistical results. The average tumor weight was also significantly minor in the LIUS and MBs treatment group compared with the control group (Fig. 2F, G). In summary, the results suggested that LIUS and MBs treatment decreased tumorigenicity and metastatic potential of ovarian cancer *in vivo*.

3.3 LIUS combined with MBs reduced ovarian cancer metastasis in an intraperitoneal and hematogenous model

Transcoelomic metastasis and hematogenous metastasis are two main metastatic routes for ovarian cancer [17, 38]. To investigate the impact of LIUS and MBs treatment on ovarian cancer metastasis we constructed peritoneal metastasis and hematogenous metastasis mouse models. SKOV3 cells which were treated after LIUS and MBs and then these were used to form peritoneal and

hematogenous metastases models (Fig. 3A, B). Bioluminescent imaging demonstrated that the cell metastasis ability had decreased after LIUS and MBs treatment, especially in the hematogenous metastasis model (Fig. 3C, D). In this study, there were notably less peritoneal metastases in the peritoneal tumor transplant models after treatment with LIUS and MBs (Fig. 3C, Fig. S5A), and almost no metastatic tumors in the lung after caudal vein injection compared to the control group (Fig. 3D, Fig. S5B). The average total luminescence flux in nude mice was also quantitatively analyzed, with a significant decrease observed in the LIUS and MBs treatment group compared to the control group. The differences for the caudal vein injection nude mice was even more obvious (Fig. 3E, F) (for peritoneal metastases: Day10: 2.37e8 ± 1.36e8 *vs* 1.01e8, p=0.014; Day17: 6.67e8 ± 3.91e8 *vs* 2.76e8 ± 2.22e8, p=0.0064; Day24: 9.36e8 ± 6.21e8 *vs* 5.88e8 ± 6.29e8, p=1863; Day31: 1.61e9 ± 1.32e9 *vs* 5.42e8 ± 5.72e8, p=0.0225) (for hematogenous metastasis: Day10: 4.56e5 ± 1.74e5 *vs* 2.11e5 ± 1.05e5, p<0.001; Day17: 6.79e5 ± 2.85e5 *vs* 4.67 ± 1.39e5, p<0.001; Day24: 9.68e5 ± 6.36e5 *vs* 3.41e5 ± 1.72e5, p<0.001; Day31: 1.36e6 ± 9.38e5 *vs* 4.26e5 ± 3.41e5, p<0.001). Over time, SKOV3 cells treated with LIUS and MBs demonstrated a gradual progression of abdominal lesions in the peritoneal tumor transplant model, whereas no significant progression was observed in the hematogenous metastatic model. For the inoculated tumors observed on day 31, macroscopic observation revealed that the total number of tumor nodes were lower in the LIUS and MBs treatment group (Fig. 3G-H). The number of metastatic lesions significantly decreased in LIUS + MBs treatment group (intraperitoneally metastasis: 2.83 ± 1.33 *vs* 1.33 ± 0.52, p=0.028) (lung metastasis: 4.75 ± 1.71 *vs* 0.33 ± 0.52, p<0.001), particularly in the hematogenous metastatic model. This same observation was even more obvious in hematogenous metastasis nude mice (Fig. 3I-J). Representative HE staining were shown in the Fig. S6A, B. These findings suggested that LIUS and MBs treatment had diminished the ovarian cancer cell metastatic potential *in vivo,* especially the hematogenous metastatic model.

3.4 LIUS combined with MBs disrupted the formation and protrusion of filopodia

Filopodia and lamellipodia on the edge of the cell are essential for cell migration, allowing it to move forward [39, 40]. Thus, the formation of filopodia plays a critical role in cell invasion [41]. To elucidate the cellular mechanisms underlying the inhibition of ovarian cancer metastasis following LIUS and MBs treatment, resultant alterations in filopodia and lamellipodia were

evaluated. Scanning electron microscopy observations of filopodia and lamellipodia in SKOV3 cells are shown in Fig. 4A. Filopodia are slender, elongated structures extending from the cell membrane, while lamellipodia are sheet-like protrusions on the cell surface, both composed of F-actin [42, 43]. According to the scanning electron microscope image, after LIUS and MBs treatment, the filopodia was almost invisible, but the lamellipodia was still visible. The changes of F-actin filopodia and lamellipodia were analyzed through immunofluorescence staining (Fig. 4B). Through specific staining of F-actin, LIUS and MBs treatment cells showed less (4.093 ± 1.513 *vs* 1.265 ± 0.8956, $p<0.001$) and shorter (6.408 ± 2.255 *vs* 3.250 ± 1.602, $p<0.001$) F-actin filopodia (Fig. 4C, D). Interestingly, there was no statistically significant differences (3.333 ± 0.7112 vs 3.167 ± 0.9499, $p=0.445$) observed in the F-actin lamellipodia following LIUS and MBs treatment (Fig. 4E). This data therefore indicated that LIUS and MBs treatment inhibited the formation and protrusion of filopodia, but had no effect on lamellipodia. Collectively, our results suggest LIUS and MBs treatment has the potential to impede cell invasion and migration in ovarian cancer primarily by inhibiting the formation of filopodia.

3.5 LIUS combined with MBs suppressed Cdc42 activity

The small GTPase Cdc42 is well known to participate in the process of cell migration [44]. As Cdc42 is required for filopodia formation, achieved via its stimulation of downstream effector proteins [19, 20]. This study attempted to investigate whether alterations in Cdc42 participated in remodeling the filopodia after LIUS and MBs treatment. For this, we employed RNA sequencing to quantify Cdc42 mRNA levels at various time points following LIUS and MBs treatment. However, the findings indicated that the overall expression of Cdc42 mRNA remained unaltered after LIUS and MBs treatment 3h, 6h, 12h, and 24h (Fig. 5A). Moreover, quantitative proteomic analysis revealed that 6h, 12h, and 24h after LIUS and MBs treatment did not affect the protein levels of Cdc42 (Fig. 5B). Cdc42, a member of the Rho family small GTPases, functions as a molecular switch, governing the conversion between its inactive form (Cdc42-GDP) and active form (Cdc42-GTP). It is well-established that the diverse functions of small GTPases are regulated through interactions with key regulators, including guanine nucleotide exchange factors (GEFs) and GTPase-activating proteins (GAPs) [45-47]. We investigated whether LIUS and MBs inhibit the development and extension of filopodia by modulating Cdc42 activity in SKOV3 cells. Proteomic

analysis of SKOV3 cells treated with LIUS and MBs revealed differential regulation of GEFs and GAPs involved in Cdc42 modulation. Additionally, protein-protein interactions were observed (Fig. 5C). Proteomic heat map analysis revealed that, after LIUS and MBs treatment, GEFs (RhoGEF1, 2, 7, 10, 18) and GAPs (RhoGAP1, 12, 17, 29, 35) formed small clusters, with a significant increase at 6 hours, followed by a gradual decrease at 12 and 24 hours (Fig. 5D, E). It is suggested that LIUS and MBs treatment induces complex regulatory processes within the SKOV3 cells, which may influence the activity of CDC42. The total cellular level of Cdc42 protein, regardless of treatment with LIUS and MBs remained nearly unchanged as confirmed by western blot analysis. To test whether LIUS and MBs treatment affected the activation status of Cdc42, Cdc42GTP levels were measured before and after LIUS and MBs treatment. The data demonstrated a dramatic decrease in active Cdc42 resulting from LIUS and MBs treatment compared with the controlled group (Fig. 5F). Active Cdc42 can transmit the signal to the downstream cascades promote filopodia formation and mediate cell motility [48]. The findings suggested that LIUS and MBs could regulate Cdc42 activity and lead to the decrease of Cdc42 activity (Fig. 5G).

3.6 Cdc42CA rescued the migration and invasion via filopodia formation in LIUS combined with MBs treated SKOV3 cells

In cancer, the activation of Cdc42 is frequently linked to aggressive characteristics such as enhanced cell movement and invasion [49]. To elucidate if Cdc42 activity was crucial to the filopodia suppressor function of LIUS combined with MBs treatment, Cdc42CA overexpression was then applied to in SKOV3 cells (Fig. 6B). The decreased filopodia number and length by LIUS combined with MBs exposure was indeed rescued by Cdc42CA overexpression (Fig. 6A). These data demonstrated that LIUS combined with MBs treatment suppresses the formation of filopodia by preventing Cdc42 activation in SKOV3 cells (Fig. 6C, D). To assess whether LIUS and MBs-mediated Cdc42 activation affected cell migration and invasion, we examined the migration and invasion abilities of SKOV3 cells following the overexpression of Cdc42CA. The results of the wound healing assay showed that overexpression of Cdc42CA enhanced the migration of SKOV3 cells. LIUS combined with MBs treatment can inhibit this enhancement. However, the inhibitory effect of LIUS and MBs is rescued by the overexpression of CDC42CA (Fig. 6E). In the transwell migration (Fig. 6F) and invasion (Fig. 6G) assay were also performed to explore the migration and

invasion ability of SKOV3 cells upon overexpression of Cdc42CA. Again, we found that the migration and invasion ability of SKOV3 cells was significantly increased after overexpressing Cdc42CA. To investigate if Cdc42 was crucial to the metastasis suppressor function of LIUS combined with MBs, the inhibited SKOV3 cells migration and invasion via LIUS combined with MBs exposure was examined under Cdc42CA overexpression. In the transwell assay such suppression via LIUS combined with MBs treatment was then confirmed to be negated and migration and invasion properties confirmed to be rescued via Cdc42CA overexpression (Fig.6F, G). These data showed that the negation of LIUS combined with MBs of Cdc42 is critical to LIUS combined with MBs induced SKOV3 cell migration and invasion reduction.

4. Discussion

LIUS and MBs is regarded as an adjuvant therapy for cancer [13, 50]. Experimental data from numerous *in vivo* and *in vitro* studies has demonstrated the synergistic effect when LIUS and MBs treatment is incorporated with other treatments where enhanced effectiveness (from 20-80%), inhibition of tumor metastasis, and extended survival are all noted in animal models [51, 52]. Clinical studies (NCT03458975, NCT03199274, NCT03385200) on patients with unresectable liver cancer, liver metastases, and breast cancer have also exhibited promising results. In this study, the LIUS treatment device was custom-designed and built by our team, with the parameters carefully optimized to prevent damage to normal cells while generating sufficient intensity to induce Cdc42 activation, thereby inhibiting filopodia-mediated tumor metastasis.

Over recent years, significant attention has been directed towards research upon mechanisms of tumor effectiveness including aspects of apoptosis [53], tumor vascular shutdown [54], immune response [55, 56], cellular drug uptake [57], and techniques that direct permanent damage to cancer cells [58, 59], all of which are potentially impacted by LIUS and MBs treatment. Recently, Itziar González et al. reported that ultrasound irradiation inhibited pancreatic cancer cell migration in monolayer *in vitro* experiments. Their study indicates that ultrasound's impact on tumor cell invasion may result from direct mechanical forces or cavitation [15]. In this study, we utilized three distinct models: orthotopic, intraperitoneal metastatic, and hematogenous metastatic nude mouse models, to assess the spatiotemporal effects of LIUS and MBs on ovarian cancer metastasis *in vivo*. Compared to the intraperitoneal metastatic model, the results demonstrated a more pronounced

inhibitory effect of LIUS and MBs in both the orthotopic and hematogenous metastatic models. The tumor in the orthotopic model is likely confined to the ovary, representing an early stage of ovarian cancer. Moreover, repeated administration of LIUS and MB treatments appears to exert a cumulative inhibitory effect on tumor metastasis. These findings suggest a potential therapeutic strategy for early-stage ovarian cancer or for managing unresectable residual lesions post-surgery in clinical settings. LIUS and MBs exposure significantly reduced the ability of SKOV3 cells to traverse the bloodstream, although the effect on abdominal cavity implantation was relatively modest. This may be attributed to the cytotoxic activity of innate immune cells in the bloodstream targeting SKOV3 cells following treatment with LIUS and MBs. This indicated that the combination of LIUS and MBs in immunotherapy may have a synergistic effect in inhibiting ovarian cancer metastasis. Collectively, these findings highlight the promising potential of combining LIUS and MBs as an effective therapeutic strategy for inhibiting ovarian cancer metastasis, particularly in early-stage disease and in cases with residual lesions following surgery. Moreover, combining with other treatments, such as immunotherapy, may lead to enhanced therapeutic outcomes.

A few previous studies have associated LIUS and MBs stimulation with effects upon intracellular fine structures and endogenous gene/protein expression [22, 37, 60], with a particular focus upon clarifying the mechanisms underlying the inhibition of cancer metastasis. In this, the increased number of filopodia in tumor cells has been recognized as a critical characteristic of disease progression, as reported in studies ranging from those from ovarian cancer, breast cancer, small cell lung cancer, to colon cancer [61, 62]. The core structure of filopodia, the F-actin cytoskeleton, is essential for processes such as cell motility, invasion, and metastasis [41]. The F-actin cytoskeleton functions as a mechanosensitive sub-cellular organelle. LIUS and MBs stimulates cycles of stretch and release in the cell membranes and in the cytoskeleton. These can activate mechano-sensitive proteins and/or increase membrane permeability [28, 63, 64]. In this study, we observed a decrease in filopodia length and quantity after LIUS and MBs treatment. This could potentially contribute to the suppression of tumor metastasis. These findings suggested that LIUS and MBs treatment, mediated by the regulation of the cytoskeleton, may induce alterations in the morphology and quantity of filopodia. Despite this, it was interesting that the number of lamellipodia remained constant. This may be due to the ultrasound intensity being insufficient to induce changes in

lamellipodia. Alternatively, lamellipodia may be insensitive to the mechanical stimuli caused by LIUS-induced MBs oscillations.

At the molecular level, we conducted an in-depth investigation of Cdc42, a key regulator of filopodia [65]. Our findings indicated that while the expression levels of Cdc42 remained unchanged at both the transcriptional and protein levels, there was a notable reduction in its active form. The activity of Cdc42 proteins is determined by the GTP/GDP binding state as regulated by the guanine nucleotide exchange factors (GEFs)/GTPase-activating proteins (GAPs) [66-69]. When Cdc42 is activated thus facilitating the activation of the downstream cytoskeletal proteins or regulatory proteins. This subsequently promotes actin polymerization [70, 71]. Our results of the inhibition of filopodia formation were therefore attributable to a decrease in active Cdc42. In this investigation, this was particularly confirmed where the over expression Cdc42CA could partially restore the length and number of filopodia, as well as the ability of cell migration and invasion after LIUS and MBs treatment. Taken together, this study strongly supports the understanding that LIUS and MBs may impede the formation and protrusion of filopodia through the inhibition of Cdc42 activity, thereby ultimately suppressing the metastasis of ovarian cancer. The interaction between LIUS and MBs induces a moderate degree of MBs deformation, which is unlikely to cause significant direct damage to cells or DNA, but may influence post-translational modifications of proteins, such as phosphorylation. Further investigation into the more complex mechanisms underlying tumor inhibition by LIUS and MBs is warranted. This seems likely as derived from the results of this present study, where LIUS and MBs treatment potentially inhibited the formation of filamentous pseudopodia by downregulating Cdc42 activity, thereby achieving the desired effect of impeding ovarian cancer metastasis. Overall, in this study we present evidence for a novel mechanism of LIUS and MBs treatment for the inhibition of ovarian cancer metastasis.

Despite the novelty of our findings, several important issues remain to be addressed. The sample size in this study is limited, particularly with regard to in orthotopic models. Additionally, the relatively short observation period and the low incidence of metastases in the untreated group may limit the ability to draw more robust conclusions. More animal models and longer observations, as well as multiple animals, are needed to further validate the role of LIUS+MBs in inhibiting ovarian cancer metastasis in future studies. While LIUS and MBs hold promise as adjunct therapies for

tumors, there are still several challenges that need to be resolved before they can be widely translated into clinical practice. As a form of physical stimulation, ultrasound can induce a broad range of bioeffects. Warranting further investigation should focus on understanding the mechanisms underlying signal transduction via mechanical stimulation of cell membranes, as well as the intercellular communication processes involved. Moreover, the bioeffects of ultrasound may vary depending on specific parameters, and the findings of this study, which were conducted in nude mice, may not be directly applicable to humans without adjustments to the experimental parameters. Additionally, the deep location of the ovaries and the complexity of surrounding tissues present significant challenges, particularly when dealing with residual lesions that are not amenable to surgical resection. Developing strategies to inhibit tumor metastasis while sparing normal tissues remains a critical issue to be addressed in future research.

5. Conclusions

This study validated the inhibitory effect of LIUS combined with MBs on ovarian cancer metastasis using three models: the orthotopic ovarian cancer model, the abdominal metastasis model, and the hematogenous metastasis model. This inhibitory effect on the metastasis of ovarian cancer cells is achieved by altering the morphology and function of filopodia through the inhibition of Cdc42 activity via LIUS combined with MBs treatment (Fig.7). In general, this approach holds promise for the targeted inhibition of unresectable ovarian cancer and may be applicable to other tumor types, thereby offering new strategies for the clinical treatment of metastasis.

CRediT authorship contribution statement

XL: Conceptualization, methodology, data curation, formal analysis, funding acquisition, writing-original draft. **CT**: visualization, formal analysis. **XF**: western blot, formal analysis. **JQ**: SEM, methodology, funding acquisition. **WS**: investigation. **ZX**: validation. **XW**: conceptualization, methodology. **YZ**: Conceptualization, methodology, writing-review and editing. **XL**: conceptualization. **LS**: conceptualization. **JQ**: conceptualization, methodology, writing-review and editing, funding acquisition.

Funding

This work was supported by the Natural Foundation Exploration Project of Zhejiang Province (LY22H180009), the National Natural Science Foundation of China (82471986, 82171939, W2421099, and 82202158), the Medical and Health research project of Zhejiang Province (2022KY357).

Declaration of competing interest

The authors declare that they have no known competing financial interests or personal relationships that could have appeared to influence the work reported in this paper.

Data availability

Data will be made available on request.

Ethics approval and consent to participate

All experiments involving animals were conducted according to the ethical policies and procedures approved by the Ethical Committee of the Zhejiang Chinese Medical University Laboratory Animal Research Center (No. 20230911-11).

References

[1] R.L. Siegel, A.N. Giaquinto, A. Jemal, Cancer statistics, 2024, CA Cancer J Clin, 74 (2024) 12-49.

[2] D. Jiang, Z. Niu, X. Tan, H. He, L. Ren, J. Shen, X. Zhu, P. Zhao, M. Liu, H. Chen, R. Wang, Q. Li, G. Cao, The mortalities of female-specific cancers in China and other countries with distinct socioeconomic statuses: A longitudinal study, J Adv Res, 49 (2023) 127-139.

[3] D.K. Armstrong, R.D. Alvarez, J.N. Bakkum-Gamez, L. Barroilhet, K. Behbakht, A. Berchuck, L.M. Chen, M. Cristea, M. DeRosa, E.L. Eisenhauer, D.M. Gershenson, H.J. Gray, R. Grisham, A. Hakam, A. Jain, A. Karam, G.E. Konecny, C.A. Leath, J. Liu, H. Mahdi, L. Martin, D. Matei, M. McHale, K. McLean, D.S. Miller, D.M. O'Malley, S. Percac-Lima, E. Ratner, S.W. Remmenga, R.

566 Vargas, T.L. Werner, E. Zsiros, J.L. Burns, A.M. Engh, Ovarian Cancer, Version 2.2020, NCCN
567 Clinical Practice Guidelines in Oncology, J Natl Compr Canc Netw, 19 (2021) 191-226.
568 [4] T. Sun, Z. Zhang, L. Tian, Y. Zheng, L. Wu, Y. Guo, X. Li, Y. Li, H. Shen, Y. Lai, J. Liu, H. Cui,
569 S. He, Y. Ren, G. Yang, Dualistic classification of high grade serous ovarian carcinoma has its
570 root in spatial heterogeneity, J Adv Res, 48 (2023) 213-225.
571 [5] K. Kooiman, S. Roovers, S.A.G. Langeveld, R.T. Kleven, H. Dewitte, M.A. O'Reilly, J.M.
572 Escoffre, A. Bouakaz, M.D. Verweij, K. Hynynen, I. Lentacker, E. Stride, C.K. Holland, Ultrasound-
573 Responsive Cavitation Nuclei for Therapy and Drug Delivery, Ultrasound Med Biol, 46 (2020)
574 1296-1325.
575 [6] I. Lentacker, I. De Cock, R. Deckers, S.C. De Smedt, C.T. Moonen, Understanding ultrasound
576 induced sonoporation: definitions and underlying mechanisms, Adv Drug Deliv Rev, 72 (2014)
577 49-64.
578 [7] Z. Lin, L. Meng, J. Zou, W. Zhou, X. Huang, S. Xue, T. Bian, T. Yuan, L. Niu, Y. Guo, H. Zheng,
579 Non-invasive ultrasonic neuromodulation of neuronal excitability for treatment of epilepsy,
580 Theranostics, 10 (2020) 5514-5526.
581 [8] Y. Zhang, N. Tang, L. Huang, W. Qiao, Q. Zhu, Z. Liu, Effect of diagnostic ultrasound and
582 microbubble-enhanced chemotherapy on metastasis of rabbit VX2 tumor, Med Phys, 48 (2021)
583 3927-3935.
584 [9] B. Kip, C.U. Tunc, O. Aydin, Triple-combination therapy assisted with ultrasound-active gold
585 nanoparticles and ultrasound therapy against 3D cisplatin-resistant ovarian cancer model,
586 Ultrason Sonochem, 82 (2022) 105903.
587 [10] N. Hosano, Z. Moosavi-Nejad, T. Hide, H. Hosano, Focused shock waves and inertial

588 cavitation release tumor-associated antigens from renal cell carcinoma, Ultrason Sonochem,
589 (2024) 107078.
590 [11] H. Zhou, C. Zhu, Q. Zhao, J. Ni, H. Zhang, G. Yang, J. Ge, C. Fang, H. Wei, X. Zhou, K.
591 Zhang, Wrecking neutrophil extracellular traps and antagonizing cancer-associated
592 neurotransmitters by interpenetrating network hydrogels prevent postsurgical cancer relapse and
593 metastases, Bioact Mater, 39 (2024) 14-24.
594 [12] S. Kotopoulis, G. Dimcevski, O.H. Gilja, D. Hoem, M. Postema, Treatment of human
595 pancreatic cancer using combined ultrasound, microbubbles, and gemcitabine: a clinical case
596 study, Med Phys, 40 (2013) 072902.
597 [13] G. Dimcevski, S. Kotopoulis, T. Bjånes, D. Hoem, J. Schjott, B.T. Gjertsen, M. Biermann, A.
598 Molven, H. Sorbye, E. McCormack, M. Postema, O.H. Gilja, A human clinical trial using
599 ultrasound and microbubbles to enhance gemcitabine treatment of inoperable pancreatic cancer,
600 J Control Release, 243 (2016) 172-181.
601 [14] Y.J. Wang, Y. Li, K. Yan, L. Shen, W. Yang, J.F. Gong, K. Ding, Clinical study of ultrasound
602 and microbubbles for enhancing chemotherapeutic sensitivity of malignant tumors in digestive
603 system, Chinese J Cancer Res, 30 (2018) 553-563.
604 [15] I. Gonzalez, J. Luzuriaga, A. Valdivieso, M. Candil, J. Frutos, J. Lopez, L. Hernandez, L.
605 Rodriguez-Lorenzo, V. Yague, J.L. Blanco, A. Pinto, J. Earl, Low-intensity continuous ultrasound
606 to inhibit cancer cell migration, Front Cell Dev Biol, 10 (2022) 842965.
607 [16] D.X. Nguyen, P.D. Bos, J. Massague, Metastasis: from dissemination to organ-specific
608 colonization, Nat Rev Cancer, 9 (2009) 274-284.
609 [17] M. Yousefi, S. Dehghani, R. Nosrati, M. Ghanei, A. Salmaninejad, S. Rajaie, M. Hasanzadeh,

610 A. Pasdar, Current insights into the metastasis of epithelial ovarian cancer - hopes and hurdles,
611 Cell Oncol (Dordr), 43 (2020) 515-538.
612 [18] K.M. Alblazi, C.H. Siar, Cellular protrusions--lamellipodia, filopodia, invadopodia and
613 podosomes--and their roles in progression of orofacial tumours: current understanding, Asian
614 Pac J Cancer Prev, 16 (2015) 2187-2191.
615 [19] A. Hall, Rho GTPases and the actin cytoskeleton, Science, 279 (1998) 509-514.
616 [20] S. Etienne-Manneville, Cdc42--the centre of polarity, J Cell Sci, 117 (2004) 1291-1300.
617 [21] S. Etienne-Manneville, A. Hall, Rho GTPases in cell biology, Nature, 420 (2002) 629-635.
618 [22] Y. Song, J. Chen, C. Zhang, L. Xin, Q. Li, Y. Liu, C. Zhang, S. Li, P. Huang, Mechanosensitive
619 channel Piezo1 induces cell apoptosis in pancreatic cancer by ultrasound with microbubbles,
620 iScience, 25 (2022) 103733.
621 [23] J. Du, L. Zheng, P. Gao, H. Yang, W.J. Yang, F. Guo, R. Liang, M. Feng, Z. Wang, Z. Zhang,
622 L. Bai, Y. Bu, S. Xing, W. Zheng, X. Wang, L. Quan, X. Hu, H. Wu, Z. Chen, L. Chen, K. Wei, Z.
623 Zhang, X. Zhu, X. Zhang, Q. Tu, S.M. Zhao, X. Lei, J.W. Xiong, A small-molecule cocktail promotes
624 mammalian cardiomyocyte proliferation and heart regeneration, Cell Stem Cell, 29 (2022) 545-
625 558 e513.
626 [24] J.C. Thiele, M. Jungblut, D.A. Helmerich, R. Tsukanov, A. Chizhik, A.I. Chizhik, M.J.
627 Schnermann, M. Sauer, O. Nevskyi, J. Enderlein, Isotropic three-dimensional dual-color super-
628 resolution microscopy with metal-induced energy transfer, Sci Adv, 8 (2022) eabo2506.
629 [25] Y. Werner, E. Mass, P. Ashok Kumar, T. Ulas, K. Handler, A. Horne, K. Klee, A. Lupp, D.
630 Schutz, F. Saaber, C. Redecker, J.L. Schultze, F. Geissmann, R. Stumm, Cxcr4 distinguishes
631 HSC-derived monocytes from microglia and reveals monocyte immune responses to

632 experimental stroke, Nat Neurosci, 23 (2020) 351-362.
633 [26] A.R. Young, M. Narita, M. Ferreira, K. Kirschner, M. Sadaie, J.F. Darot, S. Tavare, S. Arakawa,
634 S. Shimizu, F.M. Watt, M. Narita, Autophagy mediates the mitotic senescence transition, Genes
635 Dev, 23 (2009) 798-803.
636 [27] S. Hu, K. Meng, T. Wang, R. Qu, B. Wang, Y. Xi, T. Yu, Z. Yuan, Z. Cai, Y. Tian, C. Zeng, X.
637 Wang, W. Zou, X. Fu, L. Li, Lung cancer cell-intrinsic IL-15 promotes cell migration and sensitizes
638 murine lung tumors to anti-PD-L1 therapy, Biomark Res, 12 (2024) 40.
639 [28] E.F. Schibber, D.R. Mittelstein, M. Gharib, M.G. Shapiro, P.P. Lee, M. Ortiz, A dynamical
640 model of oncotripsy by mechanical cell fatigue: selective cancer cell ablation by low-intensity
641 pulsed ultrasound, Proc Math Phys Eng Sci, 476 (2020) 20190692.
642 [29] G. Fan, J. Qin, X. Fu, X. Si, L. Li, K. Yang, B. Wang, H. Lou, J. Zhu, Low-Intensity Focused
643 Ultrasound Targeted Microbubble Destruction Enhanced Paclitaxel Sensitivity by Decreasing
644 Autophagy in Paclitaxel-Resistant Ovarian Cancer, Front Oncol, 12 (2022) 823956.
645 [30] L. Wang, X. Li, F. Gao, Y. Liu, S. Lang, C. Wang, D. Zhang, Effect of ultrasound combined
646 with exogenous GABA treatment on polyphenolic metabolites and antioxidant activity of mung
647 bean during germination, Ultrason Sonochem, 94 (2023) 106311.
648 [31] K. Saito, K. Miyake, P.L. McNeil, K. Kato, K. Yago, N. Sugai, Plasma membrane disruption
649 underlies injury of the corneal endothelium by ultrasound, Exp Eye Res, 68 (1999) 431-437.
650 [32] T. Bjanes, S. Kotopoulis, E.T. Murvold, T. Kamceva, B.T. Gjertsen, O.H. Gilja, J. Schjott, B.
651 Riedel, E. McCormack, Ultrasound- and Microbubble-Assisted Gemcitabine Delivery to
652 Pancreatic Cancer Cells, Pharmaceutics, 12 (2020).
653 [33] M. Du, T. Wang, W. Peng, R. Feng, M. Goh, Z. Chen, Bacteria-driven nanosonosensitizer

delivery system for enhanced breast cancer treatment through sonodynamic therapy-induced immunogenic cell death, J Nanobiotechnology, 22 (2024) 167.

[34] Y. Zhao, D. Shi, L. Guo, M. Shang, X. Sun, D. Meng, S. Xiao, X. Wang, J. Li, Ultrasound targeted microbubble destruction-triggered nitric oxide release via nanoscale ultrasound contrast agent for sensitizing chemoimmunotherapy, J Nanobiotechnology, 21 (2023) 35.

[35] R.Y. Huang, Y.H. Lin, S.Y. Lin, Y.N. Li, C.S. Chiang, C.W. Chang, Magnetic ternary nanohybrids for nonviral gene delivery of stem cells and applications on cancer therapy, Theranostics, 9 (2019) 2411-2423.

[36] S. Orsulic, Y. Li, R.A. Soslow, L.A. Vitale-Cross, J.S. Gutkind, H.E. Varmus, Induction of ovarian cancer by defined multiple genetic changes in a mouse model system, Cancer Cell, 1 (2002) 53-62.

[37] Y. He, X.H. Dong, Q. Zhu, Y.L. Xu, M.L. Chen, Z. Liu, Ultrasound-triggered microbubble destruction enhances the radiosensitivity of glioblastoma by inhibiting PGRMC1-mediated autophagy in vitro and in vivo, Mil Med Res, 9 (2022) 9.

[38] S. Pradeep, S.W. Kim, S.Y. Wu, M. Nishimura, P. Chaluvally-Raghavan, T. Miyake, C.V. Pecot, S.J. Kim, H.J. Choi, F.Z. Bischoff, J.A. Mayer, L. Huang, A.M. Nick, C.S. Hall, C. Rodriguez-Aguayo, B. Zand, H.J. Dalton, T. Arumugam, H.J. Lee, H.D. Han, M.S. Cho, R. Rupaimoole, L.S. Mangala, V. Sehgal, S.C. Oh, J. Liu, J.S. Lee, R.L. Coleman, P. Ram, G. Lopez-Berestein, I.J. Fidler, A.K. Sood, Hematogenous metastasis of ovarian cancer: rethinking mode of spread, Cancer Cell, 26 (2014) 77-91.

[39] T.D. Pollard, G.G. Borisy, Cellular motility driven by assembly and disassembly of actin filaments, Cell, 112 (2003) 453-465.

[40] E.S. Chhabra, H.N. Higgs, The many faces of actin: matching assembly factors with cellular structures, Nat Cell Biol, 9 (2007) 1110-1121.

[41] G. Jacquemet, H. Hamidi, J. Ivaska, Filopodia in cell adhesion, 3D migration and cancer cell invasion, Curr Opin Cell Biol, 36 (2015) 23-31.

[42] R. Zou, W. Shi, X. Chang, M. Zhang, S. Tan, R. Li, H. Zhou, Y. Li, G. Wang, W. Lv, X. Fan, The DNA-dependent protein kinase catalytic subunit exacerbates endotoxemia-induced myocardial microvascular injury by disrupting the MOTS-c/JNK pathway and inducing profilin-mediated lamellipodia degradation, Theranostics, 14 (2024) 1561-1582.

[43] D.Y. Chen, N.H. Sun, Y.P. Lu, L.J. Hong, T.T. Cui, C.K. Wang, X.H. Chen, S.S. Wang, L.L. Feng, W.X. Shi, K. Fukunaga, Z. Chen, Y.M. Lu, F. Han, GPR124 facilitates pericyte polarization and migration by regulating the formation of filopodia during ischemic injury, Theranostics, 9 (2019) 5937-5955.

[44] N. Reymond, J.H. Im, R. Garg, F.M. Vega, B. Borda d'Agua, P. Riou, S. Cox, F. Valderrama, R.J. Muschel, A.J. Ridley, Cdc42 promotes transendothelial migration of cancer cells through beta1 integrin, J Cell Biol, 199 (2012) 653-668.

[45] K. Wennerberg, K.L. Rossman, C.J. Der, The Ras superfamily at a glance, J Cell Sci, 118 (2005) 843-846.

[46] N. Mitin, K.L. Rossman, C.J. Der, Signaling interplay in Ras superfamily function, Curr Biol, 15 (2005) R563-574.

[47] H. Farhan, V.W. Hsu, Cdc42 and Cellular Polarity: Emerging Roles at the Golgi, Trends Cell Biol, 26 (2016) 241-248.

[48] Y. He, D. Li, S.L. Cook, M.S. Yoon, A. Kapoor, C.V. Rao, P.J. Kenis, J. Chen, F. Wang,

698 Mammalian target of rapamycin and Rictor control neutrophil chemotaxis by regulating
699 Rac/Cdc42 activity and the actin cytoskeleton, Mol Biol Cell, 24 (2013) 3369-3380.
700 [49] M.D.M. Maldonado, S. Dharmawardhane, Targeting Rac and Cdc42 GTPases in Cancer,
701 Cancer Res, 78 (2018) 3101-3111.
702 [50] S. Yang, P. Wang, X.B. Wang, X.M. Su, Q.H. Liu, Activation of microbubbles by low-level
703 therapeutic ultrasound enhances the antitumor effects of doxorubicin, Eur Radiol, 24 (2014)
704 2739-2753.
705 [51] J. Qin, T.Y. Wang, J.K. Willmann, Sonoporation: Applications for Cancer Therapy, Adv Exp
706 Med Biol, 880 (2016) 263-291.
707 [52] S. Pelka, C. Guha, Enhancing Immunogenicity in Metastatic Melanoma: Adjuvant Therapies
708 to Promote the Anti-Tumor Immune Response, Biomedicines, 11 (2023).
709 [53] L. Chen, D. Cong, Y. Li, D. Wang, Q. Li, S. Hu, Combination of sonodynamic with
710 temozolomide inhibits C6 glioma migration and promotes mitochondrial pathway apoptosis via
711 suppressing NHE-1 expression, Ultrason Sonochem, 39 (2017) 654-661.
712 [54] X. Zhao, C. Pellow, D.E. Goertz, Intravital imaging and cavitation monitoring of antivascular
713 ultrasound in tumor microvasculature, Theranostics, 13 (2023) 250-266.
714 [55] A. Rix, H. Heinrichs, C. Porte, C. Leenaars, A. Bleich, F. Kiessling, Ultrasound-induced
715 immune responses in tumors: A systematic review and meta-analysis, J Control Release, 371
716 (2024) 146-157.
717 [56] J. Tang, J. Tang, H. Li, J. Zhou, N. Tang, Q. Zhu, X. Wang, B. Zhu, N. Li, Z. Liu, Mechanical
718 destruction using a minimally invasive Ultrasound Needle induces anti-tumor immune responses
719 and synergizes with the anti-PD-L1 blockade, Cancer Lett, 554 (2023) 216009.

720 [57] W.H. Liao, M.Y. Hsiao, Y. Kung, H.L. Liu, J.C. Bera, C. Inserra, W.S. Chen, TRPV4 promotes
721 acoustic wave-mediated BBB opening via Ca(2+)/PKC-delta pathway, J Adv Res, 26 (2020) 15-
722 28.
723 [58] L.B. Feril, Jr., K. Yamaguchi, Y. Ikeda-Dantsuji, Y. Furusawa, Y. Tabuchi, I. Takasaki, R.
724 Ogawa, Z.G. Cui, K. Tachibana, Low-intensity ultrasound inhibits melanoma cell proliferation in
725 vitro and tumor growth in vivo, J Med Ultrason (2001), 48 (2021) 451-461.
726 [59] T. Saliev, D. Begimbetova, D. Baiskhanova, D. Abetov, U. Kairov, C.P. Gilman, B.
727 Matkarimov, K. Tachibana, Apoptotic and genotoxic effects of low-intensity ultrasound on healthy
728 and leukemic human peripheral mononuclear blood cells, J Med Ultrason (2001), 45 (2018) 31-
729 39.
730 [60] P. Atherton, F. Lausecker, A. Harrison, C. Ballestrem, Low-intensity pulsed ultrasound
731 promotes cell motility through vinculin-controlled Rac1 GTPase activity, J Cell Sci, 130 (2017)
732 2277-2291.
733 [61] J.T. Groves, J. Kuriyan, Molecular mechanisms in signal transduction at the membrane, Nat
734 Struct Mol Biol, 17 (2010) 659-665.
735 [62] T.D. Pollard, J.A. Cooper, Actin, a central player in cell shape and movement, Science, 326
736 (2009) 1208-1212.
737 [63] X. Chen, R.S. Leow, Y. Hu, J.M. Wan, A.C. Yu, Single-site sonoporation disrupts actin
738 cytoskeleton organization, J R Soc Interface, 11 (2014) 20140071.
739 [64] B. Krasovitski, V. Frenkel, S. Shoham, E. Kimmel, Intramembrane cavitation as a unifying
740 mechanism for ultrasound-induced bioeffects, Proc Natl Acad Sci U S A, 108 (2011) 3258-
741 3263.

742 [65] C.D. Nobes, A. Hall, Rho, rac, and cdc42 GTPases regulate the assembly of multimolecular
743 focal complexes associated with actin stress fibers, lamellipodia, and filopodia, Cell, 81 (1995)
744 53-62.
745 [66] P.M. Muller, J. Rademacher, R.D. Bagshaw, C. Wortmann, C. Barth, J. van Unen, K.M. Alp,
746 G. Giudice, R.L. Eccles, L.E. Heinrich, P. Pascual-Vargas, M. Sanchez-Castro, L. Brandenburg,
747 G. Mbamalu, M. Tucholska, L. Spatt, M.T. Czajkowski, R.W. Welke, S. Zhang, V. Nguyen, T.
748 Rrustemi, P. Trnka, K. Freitag, B. Larsen, O. Popp, P. Mertins, A.C. Gingras, F.P. Roth, K. Colwill,
749 C. Bakal, O. Pertz, T. Pawson, E. Petsalaki, O. Rocks, Systems analysis of RhoGEF and RhoGAP
750 regulatory proteins reveals spatially organized RAC1 signalling from integrin adhesions, Nat Cell
751 Biol, 22 (2020) 498-511.
752 [67] H. Bagci, N. Sriskandarajah, A. Robert, J. Boulais, I.E. Elkholi, V. Tran, Z.Y. Lin, M.P. Thibault,
753 N. Dube, D. Faubert, D.R. Hipfner, A.C. Gingras, J.F. Cote, Mapping the proximity interaction
754 network of the Rho-family GTPases reveals signalling pathways and regulatory mechanisms, Nat
755 Cell Biol, 22 (2020) 120-134.
756 [68] Y.T. Zhou, L.L. Chew, S.C. Lin, B.C. Low, The BNIP-2 and Cdc42GAP homology (BCH) domain
757 of p50RhoGAP/Cdc42GAP sequesters RhoA from inactivation by the adjacent GTPase-activating
758 protein domain, Mol Biol Cell, 21 (2010) 3232-3246.
759 [69] Y. Zhou, H. Ji, Q. Xu, X. Zhang, X. Cao, Y. Chen, M. Shao, Z. Wu, J. Zhang, C. Lu, J. Yang,
760 Y. Shi, H. Bu, Congenital biliary atresia is correlated with disrupted cell junctions and polarity
761 caused by Cdc42 insufficiency in the liver, Theranostics, 11 (2021) 7262-7275.
762 [70] J. Peng, B.J. Wallar, A. Flanders, P.J. Swiatek, A.S. Alberts, Disruption of the Diaphanous-
763 related formin Drf1 gene encoding mDia1 reveals a role for Drf3 as an effector for Cdc42, Curr

764 Biol, 13 (2003) 534-545.

765 [71] M. Zhang, X. Wang, F. Guo, Q. Jia, N. Liu, Y. Chen, Y. Yan, M. Huang, H. Tang, Y. Deng, S.

766 Huang, Z. Zhou, L. Zhang, L. Zhang, Cdc42 Deficiency Leads To Epidermal Barrier Dysfunction

767 by Regulating Intercellular Junctions and Keratinization of Epidermal Cells during Mouse Skin

768 Development, Theranostics, 9 (2019) 5065-5084.

769
770
771
772
773
774
775
776
777

Figures

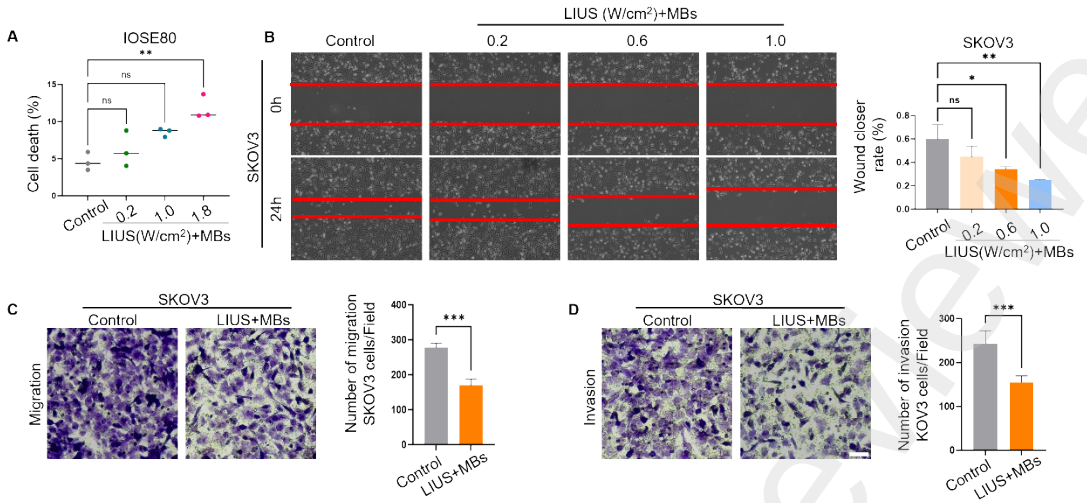

Fig.1 LIUS and MBs reduced the migration and invasion of ovarian cancer cells. (A) IOSE80 cells were treated with LIUS and MBs. The percentage of cells death was then determined using flow cytometry with Calcein AM/ propidium iodide staining, ns $p>0.05$, $^{**}p<0.01$. (B) Wound healing assays showing cell migration in SKOV3 cells. (Magnification, × 100). Quantification of the wound closer rate of SKOV3 cells, n=3, ns p>0.05, $^{*}p<0.05$, $^{**}p<0.01$. (C) Transwell migration assays in SKOV3 cells. Cells that migrated to the outer sides of the inserts were counted in five randomly selected fields, n=3, $^{***}p<0.001$. (D) Transwell invasion assays in SKOV3 cells. The cells that invaded the outer sides of the inserts were counted in five randomly selected fields, n=3, $^{***}p<0.001$.

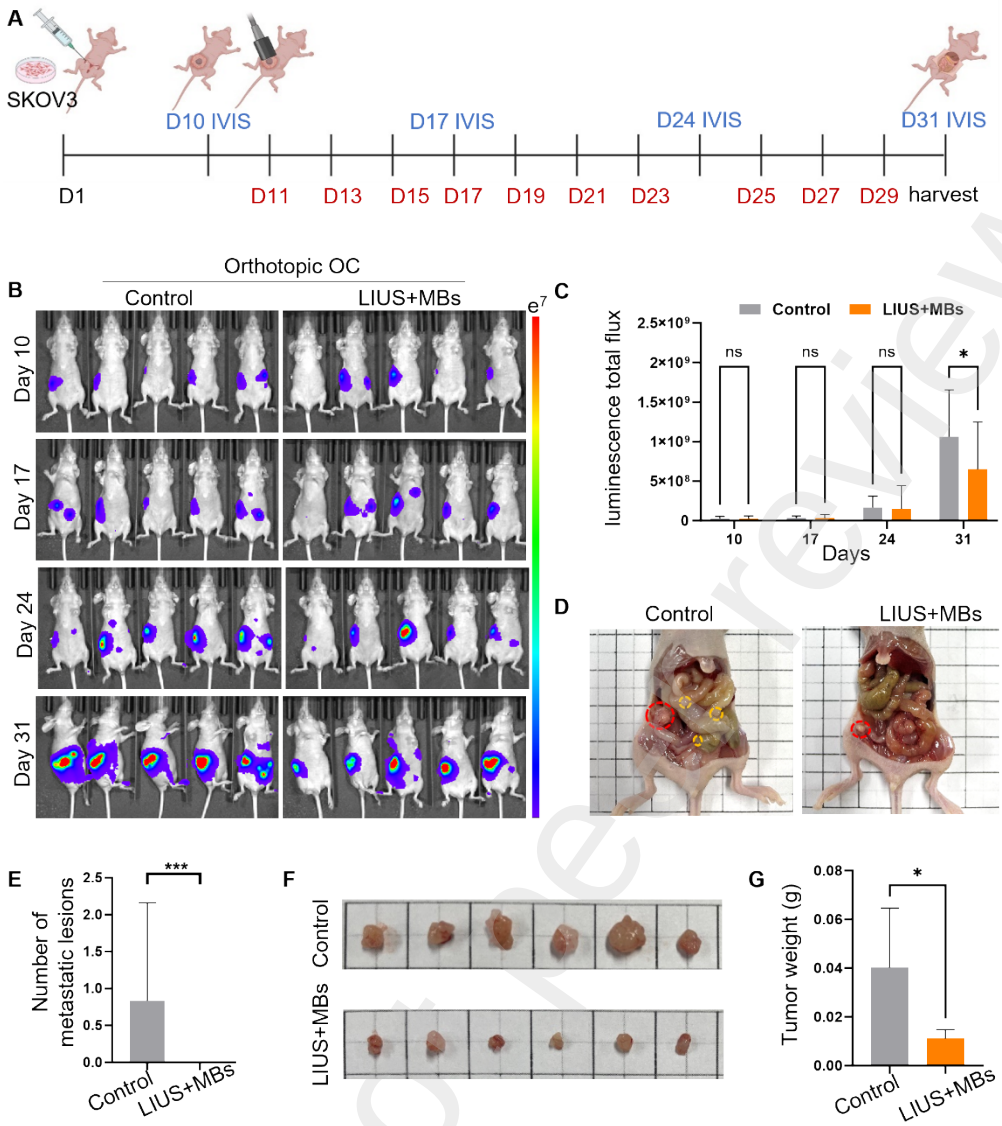

Fig.2 LIUS and MBs inhibited the tumorigenicity and metastasis in an orthotopic ovarian cancer mouse model. (A) Schema for representing the experimental procedures in the orthotopic of ovarian cancer nude mouse model. Blue letters represented IVIS imaging. Red letters represented ultrasonic cavitation treatment. (B) *In vivo* bioluminescent images of orthotopic ovarian cancer nude mouse model and quantification of bioluminescence (C), n=6, ns $p>0.05$ *$p<0.05$. (D) The macroscopic observation of the size and range of metastatic lesions in nude mice. Red circles indicate tumor in right ovary. Yellow circle indicates metastatic nodules. (E) Quantitative statistics on the number of metastatic lesions, n=6, ***$p<0.05$ (F) Representative images of tumors from the nude mice right ovary bearing xenograft tumors with SKOV3 cells treated with LIUS and MBs or without treatment. (G) The average tumor xenograft weights in nude mice, n=6. *$p<0.05$.

IVIS: *In vivo* bioluminescent images

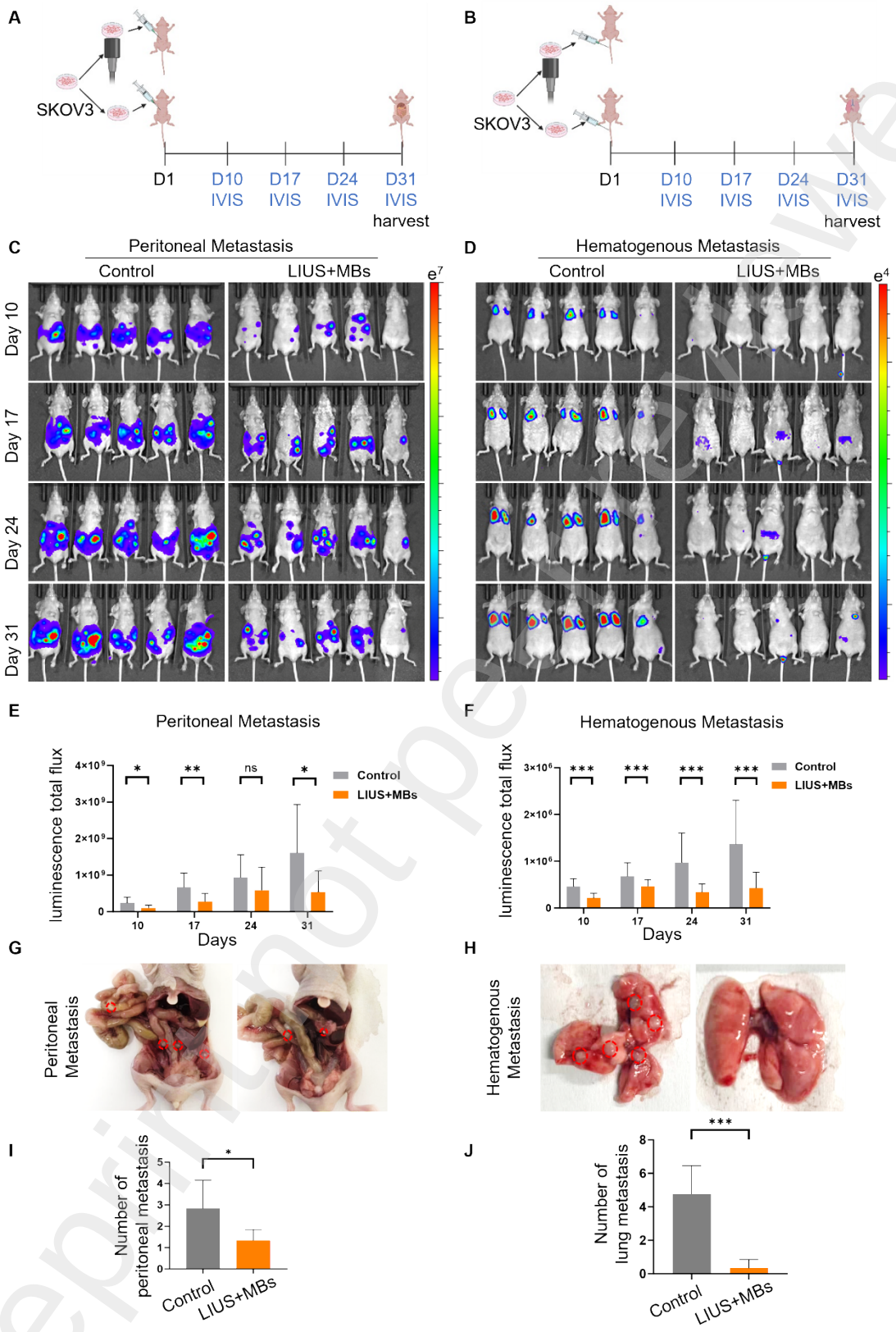

817

818 Fig.3 LIUS and MBs inhibition of ovarian cancer cells metastasis in peritoneal metastasis and
819 hematogenous metastasis nude mouse models. (A, B) Schema for representing the experimental
820 procedures. (C, D) *In vivo* bioluminescent images of peritoneal metastasis and hematogenous

metastasis of OC. (E, F) Quantification of bioluminescent in peritoneal metastasis (E) and hematogenous metastasis (F), n=6, ns $p>0.05$, $p<0.05$, $^{**}p<0.01$, $^{***}p<0.001$. (G) Macroscopic observation of the number and range of metastatic lesions in nude mice. The red circle indicates metastatic nodules. (H) Macroscopic observation of the number and range of metastatic lesions in the lungs. The red circle indicates metastatic nodules. (I) The average number of peritoneal metastatic nodules in nude mice, n=6, $^{*}p<0.05$. (J) The average number of lung metastatic nodules in nude mice, n=4-6, $^{***}p<0.001$.

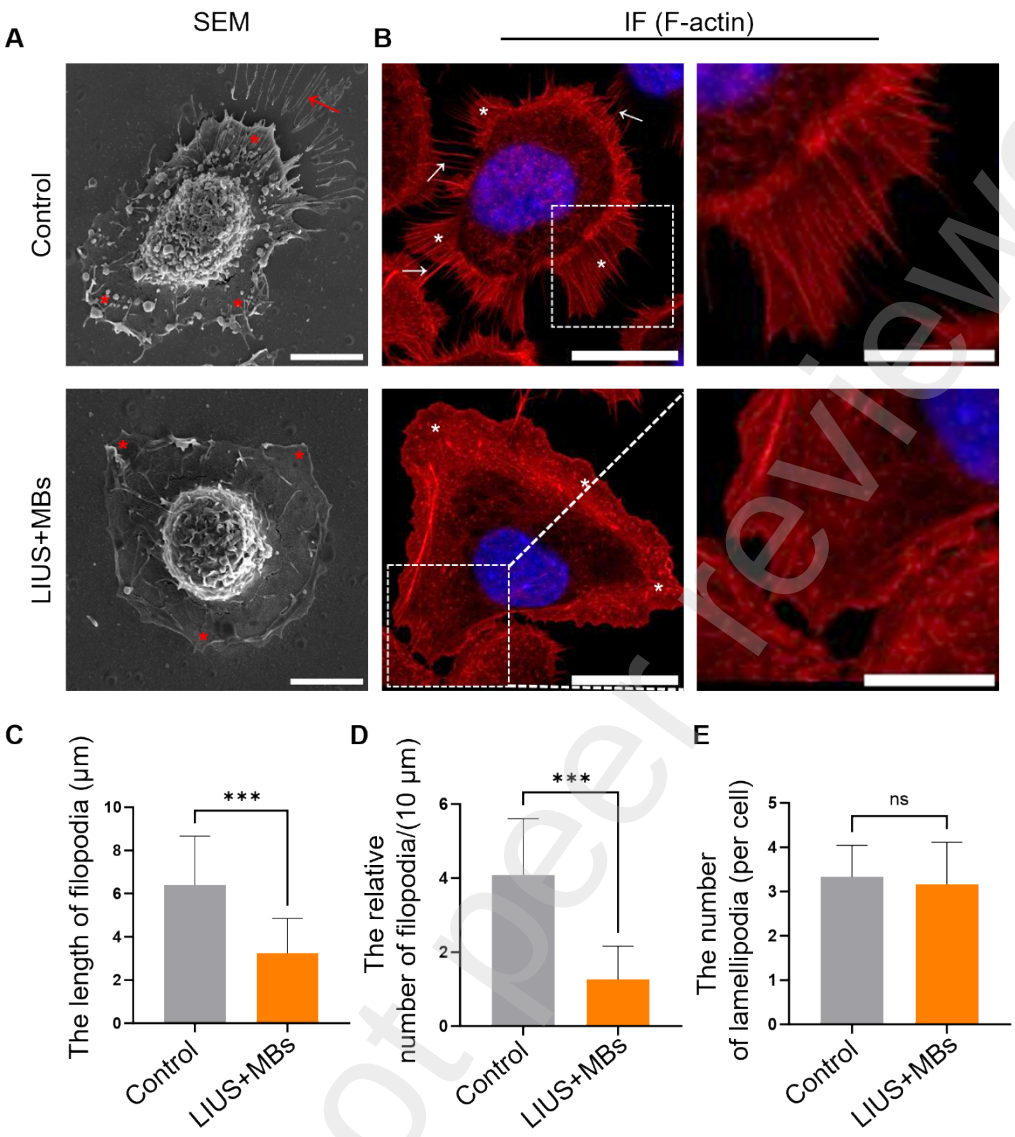

Fig.4 LIUS and MBs inhibited the formation and protrusion of filopodia. (A) SEM images of SKOV3 cells before and after LIUS and MBs treatment 6h. Red arrows show filopodia, red asterisks show lamellipodia. Scale bar = 10 μm. (B) SKOV3 cells without and with LIUS+MBs treatment for 6h where immunofluorescent staining expressing F-actin (red) images were acquired. White arrows showing filopodia, white asterisks showing lamellipodia. Scale bar: left figures at 10 μm, right figures at 5 μm. (C-E) Histograms showing the length of filopodia, number of filopodia and lamellipodia of 30 cells respectively. ***$p<0.001$, ns $p>0.05$.

SEM: scanning electron microscope. IF: immunofluorescent

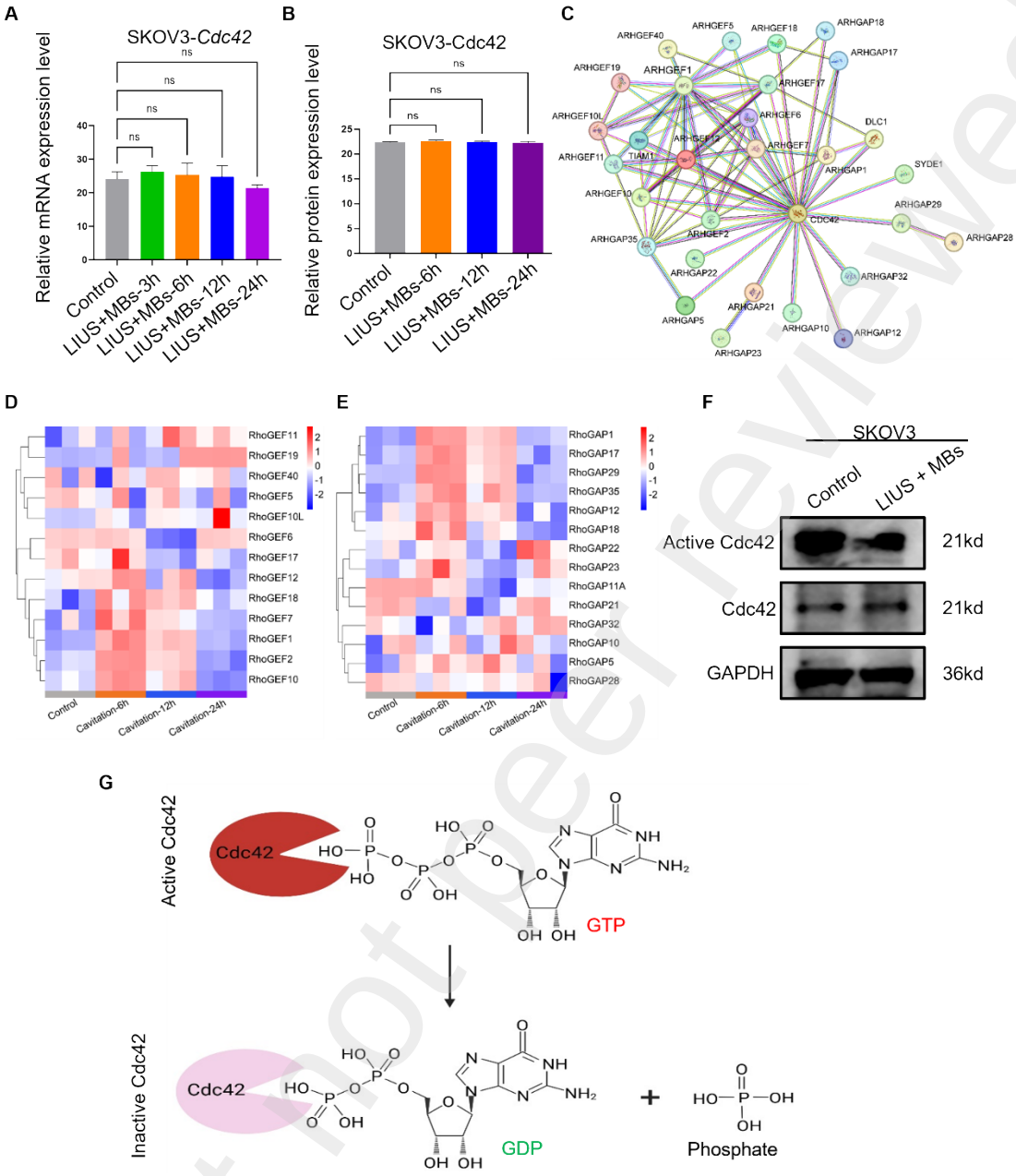

Fig.5 LIUS and MBs inhibited the activation of Cdc42 without impacting protein quantity expression. (A) Relative RNA expression level at different times of LIUS and MBs treatment. (B) Relative protein expression levels at different times of LIUS and MBs treatment. (C) RhoGAP, RhoGAP and Cdc42 interaction network. (D) Heat map of RhoGEFs expression level at different time of ultrasonic cavitation treatment. (E) Heat map of RhoGAPs expression level at different time of ultrasonic cavitation treatment. (F) Expression of Cdc42 and active Cdc42 (Cdc42GTP) both without and with LIUS and MBs treatment for 6h were analyzed by Western blot. (G) Schematic diagram of Cdc42 active and inactive transitions.

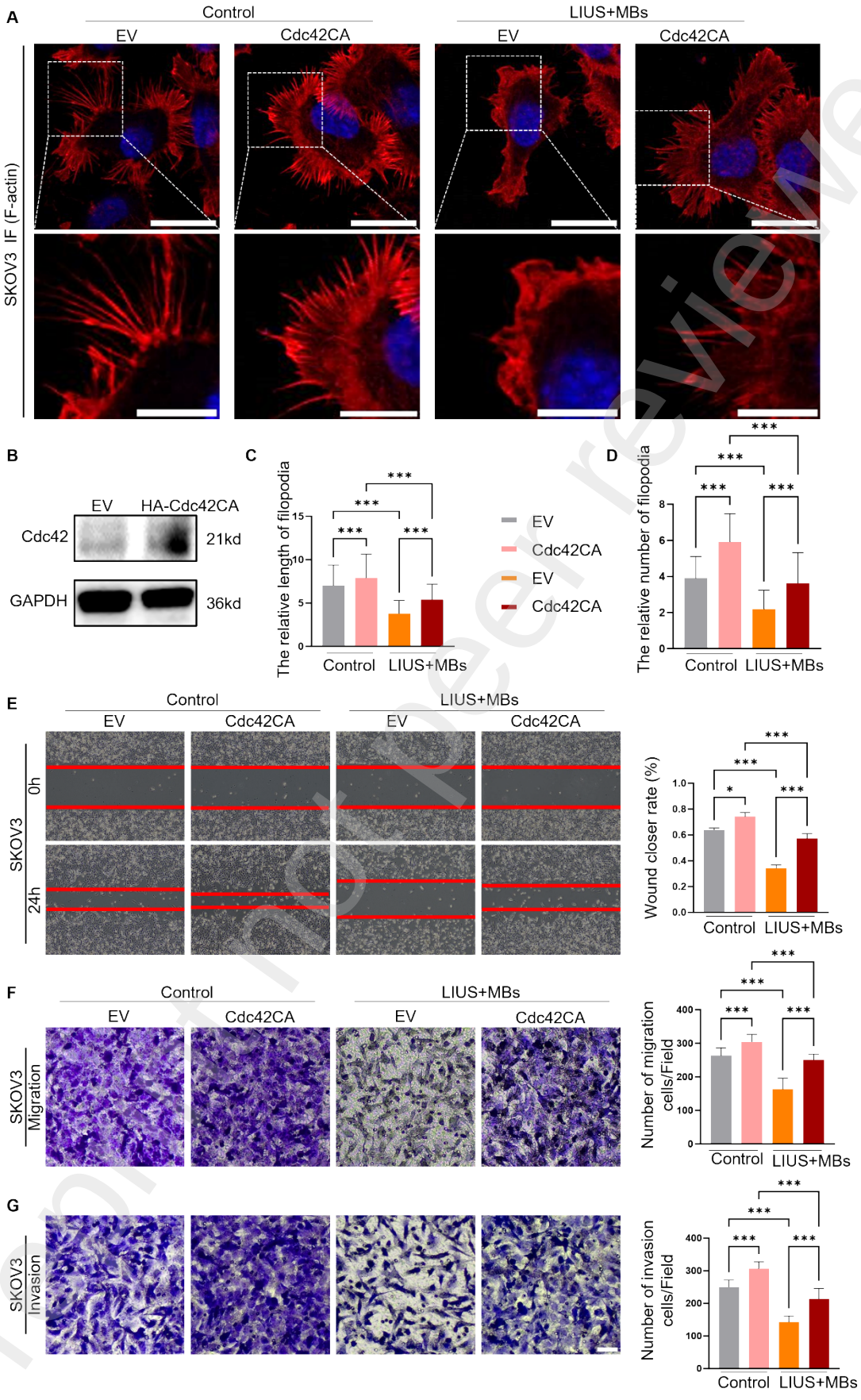

870

871 Fig.6 Overexpression Cdc42 rescues the filopodia formation and cells migration and invasion

following LIUS combined with MBs. (A) SKOV3 cells transfected with either EV or Cdc42CA plasmids, with or without LIUS and MBs treatment for 6 hours, were subjected to IF staining. (B) Expression of SKOV3 cells were transfected with empty vectors (EV) or Cdc42 constitutively activated (CA, Cdc42 G12C mutation). Histograms showing the filopodia length (C) and the number (D) of filopodia per 30 cells, respectively. *$p < 0.05$, ***$p < 0.001$. (E) Cdc42CA overexpression rescued the SKOV3 cells migration inhibition via LIUS and MBs. Quantification of the wound closer rate of SKOV3 cells. n=3, ***$p<0.001$. (F) Transwell migration assay showed that Cdc42CA overexpression rescued the inhibition of SKOV3 cell migration induced by LIUS and MBs. Quantification of the wound closer rate of SKOV3 cells. n=3, ***$p<0.001$. (G) Overexpression of Cdc42CA reversed the inhibition of SKOV3 cell invasion induced by LIUS and MBs. Quantification of the wound closer rate of SKOV3 cells. n=3, ***$p<0.001$.

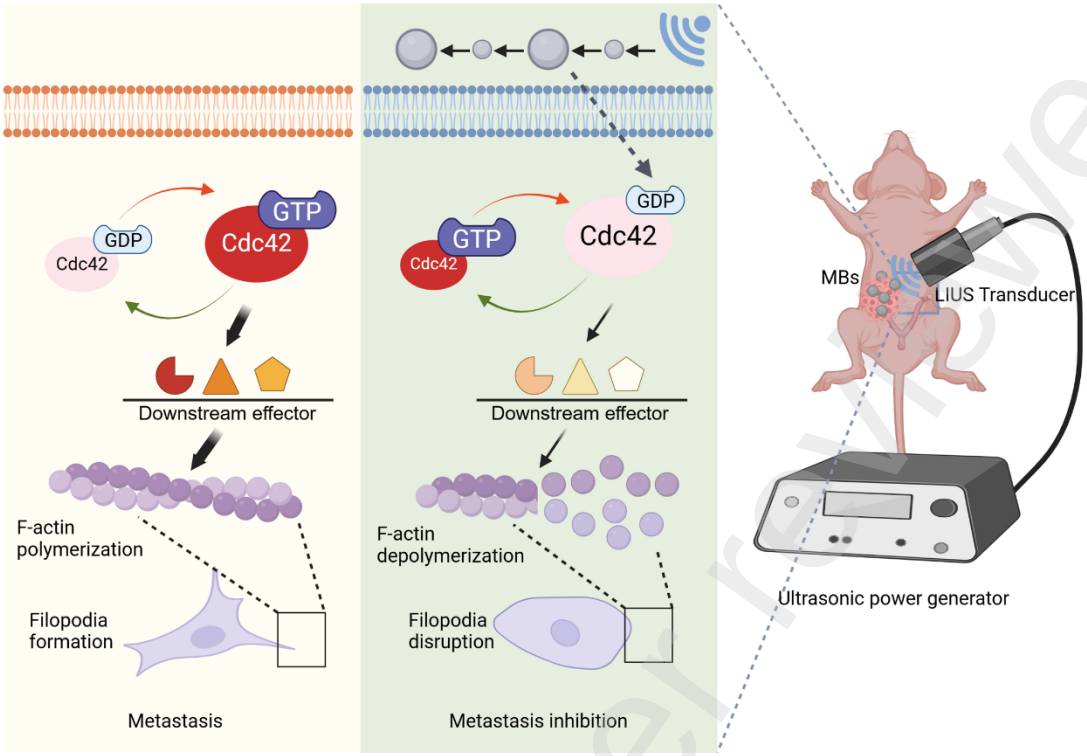

Fig.7 Schematic illustration the potential mechanism of LIUS combined with MBs inhibiting ovarian cancer metastasis. CDC42 GTPases operate as switches between inactive GDP-bound and active GTP-bound forms. In its GTP-bound state, Cdc42 activates downstream effectors, thereby inducing filopodia formation through the bundling of F-actin. LIUS and MBs treatment reduction of this activity leads to unregulated signaling finally hindering filopodia formation and inhibiting ovarian cancer metastasis.